SPACE WEATHER, VOL. 11, 95–106, doi:10.1002/swe.20019, 2013

Ensemble forecasting of coronal mass ejections using the WSA-ENLIL with CONED Model

D. Emmons,[1,2] A. Acebal,[1] A. Pulkkinen,[3,4] A. Taktakishvili,[3] P. MacNeice,[3] and D. Odstrcil[3,5]

Received 8 October 2012; revised 8 December 2012; accepted 14 December 2012; published 4 March 2013.

[1] The combination of the Wang-Sheeley-Arge (WSA) coronal model, ENLIL heliospherical model version 2.7, and CONED Model version 1.3 (WSA-ENLIL with CONED Model) was employed to form ensemble forecasts for 15 halo coronal mass ejections (halo CMEs). The input parameter distributions were formed from 100 sets of CME cone parameters derived from the CONED Model. The CONED Model used image processing along with the bootstrap approach to automatically calculate cone parameter distributions from SOHO/LASCO imagery based on techniques described by Pulkkinen et al. (2010). The input parameter distributions were used as input to WSA-ENLIL to calculate the temporal evolution of the CMEs, which were analyzed to determine the propagation times to the L_1 Lagrangian point and the maximum K_p indices due to the impact of the CMEs on the Earth's magnetosphere. The Newell et al. (2007) K_p index formula was employed to calculate the maximum K_p indices based on the predicted solar wind parameters near Earth assuming two magnetic field orientations: a completely southward magnetic field and a uniformly distributed clock-angle in the Newell et al. (2007) K_p index formula. The forecasts for 5 of the 15 events had accuracy such that the actual propagation time was within the ensemble average plus or minus one standard deviation. Using the completely southward magnetic field assumption, 10 of the 15 events contained the actual maximum K_p index within the range of the ensemble forecast, compared to 9 of the 15 events when using a uniformly distributed clock angle.

Citation: Emmons, D., A. Acebal, A. Pulkkinen, A. Taktakishvili, P. MacNeice, and D. Odstrcil (2013), Ensemble forecasting of coronal mass ejections using the WSA-ENLIL with CONED Model, *Space Weather*, *11*, 95–106, doi:10.1002/swe.20019.

1. Introduction

[2] Coronal mass ejections (CMEs) are the cause of the most severe geomagnetic storms [*Gosling*, 1993]. Geomagnetic storms can cause a variety of complications at Earth including degradation of satellite performance [*Afraimovich et al.*, 2003] and disruption of electrical systems on the Earth's surface [*Boteler et al.*, 1998]. Therefore, the space weather community has a great interest in predicting the arrival times and impacts of CMEs at Earth.

[3] A number of models have been developed to model CME propagation. Some of the earlier models include shock propagation models based on type II meter wave burst measurements such as the Shock Time of Arrival (STOA) model [*Dryer*, 1974] and the Interplanetary Shock Propagation Model (ISPM) [*Smith and Dryer*, 1990], and kinematic models based on fast and slow solar wind stream interaction such as the Hakamada-Akasofu-Fry (HAF) model [*Hakamada and Akasofu*, 1982; *Fry et al.*, 2001]. Recently, empirical forecast models have been developed, including the model developed by *Gopalswamy et al.* [2001] which treats the CME as a kinematic object experiencing accelerations or decelerations to match the ambient solar wind speed at distances near 1 AU.

[4] The most current and advanced method of forecasting CMEs is based on numerically approximating the solutions to the magnetohydrodynamic (MHD) equations governing the motion of the CME over time. ENLIL is a time-dependent three-dimensional model which solves the MHD equations for plasma mass, momentum, magnetic field, and energy density using a finite-difference approximation [*Odstrčil and Pizzo*, 1999]. ENLIL can accept the output of the Wang-Sheeley-Arge (WSA) coronal model to form the inner boundary condition in the finite-

[1]Department of Engineering Physics, Air Force Institute of Technology, Dayton, Ohio, USA.
[2]Space Vehicles Directorate, Air Force Research Laboratory, Kirtland Air Force Base, Albuquerque, New Mexico, USA.
[3]NASA Goddard Space Flight Center, Greenbelt, Maryland, USA.
[4]Catholic University of America, Washington, District of Columbia, USA.
[5]George Mason University, Fairfax, Virginia, USA.

Corresponding author: D. Emmons, Space Vehicles Directorate, Air Force Research Laboratory, Albuquerque, NM 87116, USA. (emmons29@yahoo.com)

difference computations, which calculates the background solar wind solution and interplanetary magnetic field (IMF) based on remote solar magnetogram measurements [*Arge and Pizzo*, 2000]. ENLIL can also accept the output of the Cone Model to initialize the CME speed, angular width, and axis of propagation.

[5] The Cone Model, developed by *Zhao et al.* [2002], assumes that the CME has the extent of a cone with constant angular width, propagates in a radial direction, and experiences self-similar expansion. A practical technique to manually determine the cone parameters from SOHO/LASCO imagery was developed by *Xie et al.* [2004]. Previous analyses have been completed using the analytic Cone Model along with WSA-ENLIL to forecast the impacts and propagation times of CMEs to Earth [*Odstrcil et al.*, 2004], and have showcased the effectiveness of the WSA-ENLIL with Cone Model combination [e.g., *Taktakishvili et al.*, 2009; *Taktakishvili et al.*, 2010].

[6] The analytic Cone Model relies on a manual determination of the CME outer extent from LASCO imagery. The development of the CONED Model, an automated version of the Cone Model, removed the user from the subjective process of manually determining the CME outer extent [*Pulkkinen et al.*, 2010]. The CONED Model uses image processing to automatically determine the location of the CME mass from a time-series of LASCO images and then calculates a distribution of possible cone parameters using the bootstrap approach [*Pulkkinen et al.*, 2010]. The distribution of cone parameters allows for a dynamic quantification of the uncertainty of the cone parameters based on LASCO imagery, which will vary for each event.

[7] The performance of the WSA-ENLIL with CONED Model has been analyzed with the median values of the cone parameter distributions used as input for a single WSA-ENLIL run. The *Taktakishvili et al.* [2011] analysis showed that the analytic Cone Model and CONED Model version 1.0 (automatic Cone Model) had reasonable agreement in the forecasts with a mean absolute propagation time forecast error at Earth of 6.9 h for the analytic Cone Model and 11.2 h for the CONED Model. The results of this analysis indicated that CONED Model version 1.0 required improvements to the cone parameter estimations to match the accuracy of the analytic Cone Model. The performance of the WSA-ENLIL with CONED Model version 1.2 was analyzed by *Falkenberg et al.* [2011], with the conclusion that the CME speed and angular width were underestimated by CONED Model version 1.2. CONED Model version 1.3 is the most current version of the CONED Model and has included a modification in the optimization routine to increase the CME speed and width estimations following the results of the *Falkenberg et al.* [2011] analysis.

[8] With the production of the cone parameter distributions from the CONED Model readily available, an ensemble forecast can be applied. The weather community has long known of the improvement in forecast accuracy due to the use of ensemble forecasting [*Leith*, 1974]. Ensemble forecasting also allows for a quantification of forecast uncertainty based on uncertainty in the measurements of the initial conditions, which is impossible for single forecasts. This quantification of forecast uncertainty could provide useful information to operational forecasts of CMEs.

[9] We applied the ensemble forecasting technique to 15 halo CMEs using the WSA-ENLIL with CONED Model version 1.3. The ensembles were created from 100 sets of initial states (cone parameters) derived from the CONED Model, which were used as input to WSA-ENLIL version 2.7 to obtain distributions of propagation times to the L_1 Lagrangian point and distributions of maximum K_p indices due to the impact of the CME on the Earth's magnetosphere.

2. Brief Description of WSA, ENLIL, and CONED Model

[10] In 2009, *Pulkkinen et al*. created the CONED Model, a tool which determines the cone parameters of CMEs from time series of LASCO C3 difference images automatically. The cone parameters are composed of the radial speed of the cone-front, the angular half width of the cone, the propagation axis (direction of propagation) of the cone, and the position of the CME leading edge as a function of time. The CONED Model uses image processing to automatically determine the shape of the CME mass from LASCO C3 difference images by filtering the images based on a brightness threshold, which differentiates the brighter CME mass location from the darker image background. The bootstrap approach is used to determine the confidence intervals for the calculated cone parameters by randomly selecting 300 points from the CME mass locations in the filtered LASCO images and then calculating the best-fitting cone to the randomly selected points. The process can be repeated any number of times, to create a distribution of cone parameters for the particular CME.

[11] The Wang-Sheely-Arge (WSA) model is an empirical model used to calculate background solar wind speed and IMF [*Arge and Pizzo*, 2000]. The model calculates the magnetic field between the solar surface and a boundary sphere where the magnetic field is assumed to be radial, based on synoptic magnetogram data. The solar wind speed at the boundary sphere is calculated using an inverse relationship between the solar wind speed and the magnetic expansion factor. WSA provides synoptic maps of the radial magnetic field and speed that are used by ENLIL to calculate MHD boundary conditions at 21.5 solar radii.

[12] After the input parameters are obtained from the CONED Model and the synoptic maps are obtained from the WSA model, ENLIL approximates the time-dependent solution to the MHD equations governing the plasma from 21.5 solar radii to an appropriate outer boundary (1.1 AU for quickly analyzing the effects of a CME near Earth). ENLIL utilizes a modified Total-Variation-Diminishing Lax Friedrichs (TVDLF) finite difference scheme to approximate the solution to the partial differential MHD

equations [*Tóth and Odstrcil*, 1996]. The current version of ENLIL assumes no internal magnetic field structure to the CME but allows for the distortion of the IMF by shock deflection (if a shock develops), draping around ejecta and stretching in the rarefaction region.

3. Ensemble Forecasting

[13] Formally, ensemble forecasting can be described by a transition from a probability distribution of initial states, $p(\bar{v}_t|\bar{o}_t)$, given a set of observations, $\bar{o}_t$, to a probability distribution of future states, $p(\bar{v}_{t+\tau}|\bar{o}_t)$:

$$p(\bar{v}_{t+\tau}|\bar{o}_t) = \int r(\bar{v}_{t+\tau}|\bar{v}_t)p(\bar{v}_t|\bar{o}_t)\mathrm{d}\bar{v}_t, \tag{1}$$

where $\bar{v}_t$ is the initial state, $\bar{v}_{t+\tau}$ is the future state, and $r(\bar{v}_{t+\tau}|\bar{v}_t)$ is the transition probability associated with the forecasting model [*DelSole*, 2005]. For a deterministic model (a model which provides the same result if run multiple times with the same set of initial conditions), such as ENLIL, the transition probability can be described by a delta function.

[14] The ensemble forecast distribution for a particular set of observations can be calculated from the probability distribution of future states. The ensemble forecast distribution can be statistically analyzed to obtain the most likely value of a particular parameter, along with the associated uncertainty of the value. The range of the ensemble forecast distribution provides the range of possible outcomes for a given set of observations.

[15] For this analysis, an ensemble forecast was calculated for a total of 15 halo CMEs using the WSA-ENLIL version 2.7 with CONED Model version 1.3. For each CME, the CONED Model was used to sample 100 sets of initial conditions from the probability distribution of initial states based on three LASCO C3 difference images of the CME eruption with a temporal spread of at least 1 h between the first and last images. The 100 sets of initial conditions were then used as input to WSA-ENLIL to obtain the probability distributions of future states, which were used to calculate the ensemble forecast distributions. The ensemble forecasting process used for this analysis can be summarized by

$$\begin{aligned} &\mathit{LASCO\ \ C3\ \ Difference\ \ Images} \rightarrow \bar{o}_t \rightarrow \mathit{Coned\ \ Model} \\ &\quad \rightarrow\ p(\bar{v}_t|\bar{o}_t) \rightarrow \mathit{WSA-ENLIL} \rightarrow p(\bar{v}_{t+\tau}|\bar{o}_t) \\ &\quad \rightarrow \mathit{Ensemble\ \ Forecast\ \ Distribution}. \end{aligned} \tag{2}$$

[16] Two parameters were calculated from $p(\bar{v}_{t+\tau}|\bar{o}_t)$ to obtain the ensemble forecast distributions: the propagation time of the CME to the L_1 Lagrangian point and the maximum K_p index due to the CME impact on the Earth's magnetosphere. For this analysis, the resolution of the computational grid used by ENLIL ($r \times \theta \times \phi = 160 \times 30 \times 90$) placed the L_1 Lagrangian point and Earth in the same grid cell, so the computed propagation time to Earth was the same as the computed propagation time to the L_1 Lagrangian point.

[17] The arrival time of the CME at Earth was selected to be the time at which the first temporal derivative of the solar wind dynamic pressure, calculated from ENLIL output, experienced a large increase in magnitude. The arrival time could also be considered to be the time at which the second temporal derivative of the dynamic pressure was a maximum. The arrival times computed using the first and second derivatives were compared to ensure no falsely triggered arrival times. Although not shown, the results were in good agreement.

[18] The maximum K_p indices were found using the *Newell et al.* [2007] K_p formula:

$$K_p = 0.0002947\ v^{4/3}B_T^{2/3}\sin^{8/3}(\theta_c/2) + 1, \tag{3}$$

where v is the speed (km/s) at which the IMF lines approach the magnetopause and can be approximated by the solar wind speed, B_T is the magnitude of the IMF (nT), and θ_c is the IMF clock angle defined by $\theta_c = arctan(B_y/B_z)$. The magnetic field orientation of the CME "cloud" is not computed by ENLIL, so two magnetic field orientations were assumed: First, the magnetic field was assumed to be completely southward ($\theta_c = \pi$), in order to calculate the worst-case scenario. Second, the expected value of the clock-angle term in the *Newell et al.* [2007] formula was used, assuming the clock-angle was randomly oriented with a uniform distribution. For a uniformly distributed clock-angle, the expected value of the clock-angle term was calculated to be

$$\left\langle \sin^{8/3}\left(\frac{\theta_c}{2}\right)\right\rangle = \frac{1}{2\pi}\int_0^{2\pi}\sin^{8/3}\left(\frac{\theta_c}{2}\right)\mathrm{d}\theta_c \approx 0.45. \tag{4}$$

[19] As a first-order estimation, the instantaneous (point by point) K_p was calculated from the WSA-ENLIL with CONED Model data instead of using the 6 h integration time described by *Newell et al.* [2007]. With no magnetic field orientation information available from ENLIL, the instantaneous K_p values were found to be nearly identical to the K_p values calculated using the 6 h integration time (results not shown). The K_p indices were rounded to the nearest integer value, and any calculations of the maximum K_p index using the *Newell et al.* [2007] formula exceeding nine were truncated to nine.

[20] Eight of the CMEs studied in this analysis were selected from the *Taktakishvili et al.* [2011] analysis, based on CMEs which caused particularly large geomagnetic storms. The other seven CMEs had associated maximum K_p values less than eight and had no other halo CMEs within plus or minus 2 days from the eruption day of the CME. All of the CMEs were required to have clear LASCO C3 difference images to run the CONED Model and clear ACE data to determine the actual arrival times of the CMEs at the L_1 Lagrangian point. The CMEs were also selected with a large variety of associated solar flare locations in order to analyze the performance of the model with CMEs initiated from a variety of solar locations.

Table 1. The Start Date and Times, Actual Propagation Times as Measured by ACE, Actual Maximum K_p Indices, and the Locations of the Associated Solar Flares for the 15 CMEs Analyzed. The CMEs Were Also Labeled With an Event Number for Easy Reference

Event Number	CME Start Date (Date/Month/Year)	CME Start Time (UT)	Propagation Time to ACE (HH:MM)	Maximum K_p	Associated Solar Flare Location
1	03 May 1999	06:06	56:50	3	N15E32
2	04 April 2000	16:32	47:30	9	N16W66
3	14 July 2000	10:54	27:20	9	N22W07
4	29 March 2001	10:26	37:50	9	N20W19
5	10 April 2001	05:30	33:50	8	S23W09
6	24 September 2001	10:30	33:30	7	S16E23
7	09 October 2001	11:30	52:45	6	S28E08
8	04 November 2001	16:35	32:40	9	N06W18
9	17 November 2001	05:30	60:00	4	S13E42
10	28 October 2003	11:30	18:20	9	S16E08
11	29 October 2003	20:54	19:50	9	S15W02
12	20 July 2004	13:31	44:20	7	N10E35
13	06 November 2004	02:06	39:40	9	N07E00
14	03 December 2004	00:26	54:20	4	N09E03
15	03 April 2010	10:34	45:15	8	S25E00

[21] The calculated propagation times were compared to the actual propagation times derived from ACE measurements, with 10 min resolution. The actual arrival times calculated directly from ACE data were compared to the arrival times logged in the National Oceanic and Atmospheric Administration (NOAA) Space Weather Prediction Center's (SWPC's) historical weekly reports (http://www.swpc.noaa.gov/ftpmenu/warehouse.html) to ensure consistency.

[22] The calculated maximum K_p indices were compared to the actual ground-based maximum K_p values, with integer resolution. The actual maximum K_p indices were found using NASA's OMNIWeb database (http://omniweb.gsfc.nasa.gov/form/dx1.html). The solar flare locations, derived from USAF/SOON observations, were used to approximate the location for the CME eruptions. The measured values for the actual propagation times, maximum K_p indices, and locations of the associated solar flares are displayed in Table 1.

4. Results

4.1. Single Event

[23] The ensemble distributions for event 4 (29 March 2001 CME) are displayed in this section as an example of the results obtained for each of the CMEs analyzed. The LASCO/C3 images used to create the cone parameter distributions are displayed in Figure 1, and the cone parameter distributions are displayed in Figure 2 and Table 2.

[24] Each of the 100 sets of cone parameters mapped to a separate forecast (Figure 3). The set of 100 forecasts created by the 100 sets of cone parameters formed the ensemble forecast (Figure 4). The ensemble forecast was analyzed to obtain a single forecast along with the uncertainty in the forecast, which was calculated from the width of the ensemble (Table 2). The propagation time ensemble average was used as the single forecast for the propagation time, and the rounded average (to the nearest integer) of the maximum K_p index ensemble was used as the single forecast for the maximum K_p index. The standard deviations and ranges were used to describe the width of the ensembles.

[25] For this event, the average propagation time was 36.4 h with a standard deviation of 5.8 h. With an actual propagation time of 37.8 h, the absolute forecast error (absolute value of the ensemble average minus the actual value) was 1.4 h. Using the completely southward magnetic field assumption, the average maximum K_p was calculated to be 9, with a range of 2 (the standard deviation was 0.2, which was too small to represent the uncertainty for the integer resolution used for the K_p). Using a uniformly distributed clock angle, the ensemble average was 7, with a range of 4. With an actual maximum K_p index of 9, the completely southward magnetic field predicted the magnitude perfectly, while using a uniformly distributed clock angle underestimated the magnitude by 2.

4.2. Cone Parameters

[26] The cone parameter distributions for each of the 15 CMEs are displayed in Figure 5. The 15 cone parameter distributions were averaged to obtain an overall measure of the uncertainty derived from LASCO imagery via the CONED Model (Table 3).

[27] The averages of the CONED Model speed distributions displayed a strong positive correlation with the LASCO first-order plane of sky (POS) speeds (Figure 6). The LASCO first-order POS speeds were the first-order (linear) fits to the leading edge of the CMEs in the LASCO POS imagery (http://cdaw.gsfc.nasa.gov/CME_list/) and provided an estimate of the two-dimensional POS speed of the CMEs. The strong correlation was expected because of the connection between the projected (POS) speed and the radial speed, and the fact that this analysis focused on geo-effective CMEs with a limited range of latitudes and longitudes. The average ratio of the CONED Model

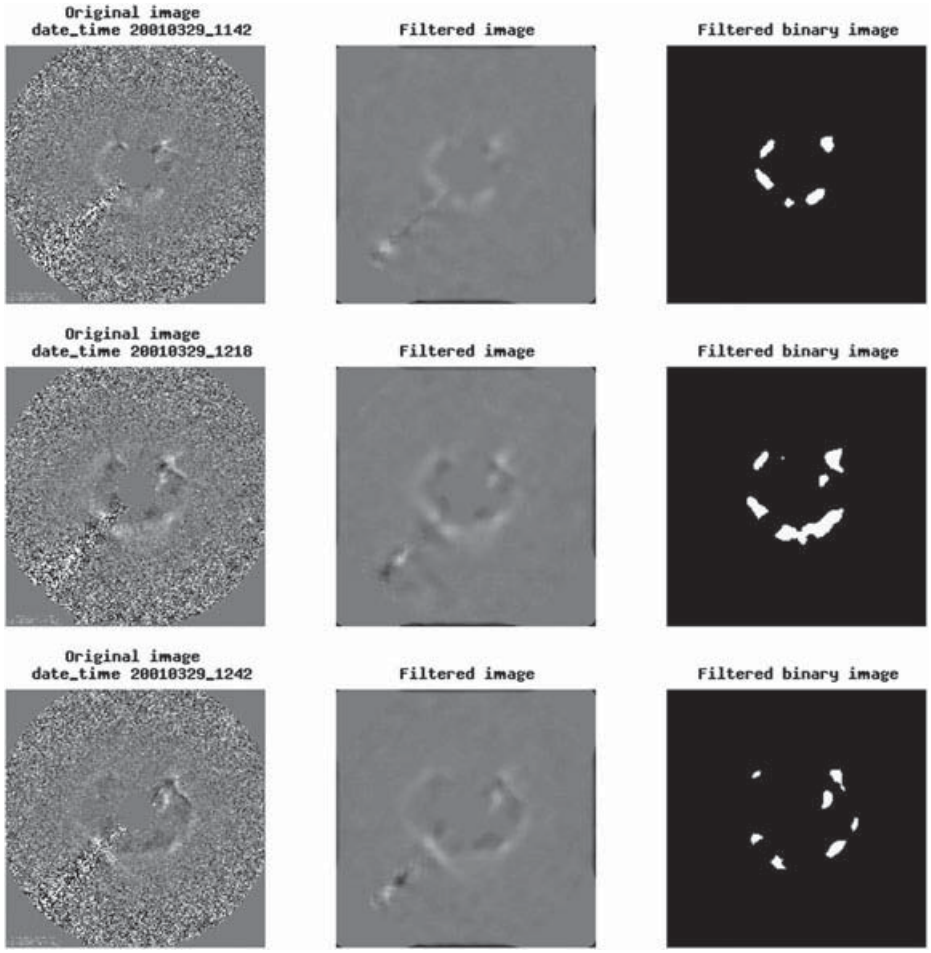

Figure 1. The LASCO C3 images used to calculate the cone parameter distributions for event 4 (29 March 2001). The format of the image time stamps follows: YYYYMMDD_HHMM. Note the 1 h time elapse from the first and last images used to calculate the cone parameter distributions.

average speeds to the LASCO first-order POS speeds was 1.2, which was consistent with the fact that the CONED Model predicted the radial (three-dimensional) speed, while the LASCO first-order POS speed was a measure of the two-dimensional POS speed. Additionally, the average ratio of the CONED Model radial speeds to the CONED Model POS speeds was calculated to be 1.1, which agreed well with the ratio of the CONED Model radial speeds to the LASCO first-order POS speeds.

[28] While the location of the associated solar flare is not necessarily an indicator of the direction of the CME propagation, the CONED Model tended to push the propagation axes of the CMEs towards the Sun-Earth line relative to the locations of the associated solar flares (Figure 7). The CONED Model calculated propagation axes with average latitude or longitude magnitudes greater than 10° for 4 of the 15 CMEs, while 13 of the 15 associated solar flare location latitude or longitude magnitudes were greater than 10°. CONED Model version 1.3 does not use the solar flare location as a constraint in the cone parameter estimations, but the results of this analysis have shown the necessity to use additional information in the calculations (efforts are currently underway to add this capability).

4.3. Propagation Time

[29] The ensemble forecasts contained 5 of the 15 actual propagation times within one standard deviation of the average (Figure 8). These five CMEs had actual propagation times between 30 and 46 h. There were two other CMEs with similar propagation times that were not forecast within one standard deviation. The actual propagation time for 8 of the 15 ensemble forecasts were within of the range of the ensemble distribution (Figure 9). Of the eight forecasts, seven were for CMEs with actual propagation times between 30 and 46 h, and the remaining forecast was for a CME with an actual propagation time around 53 h.

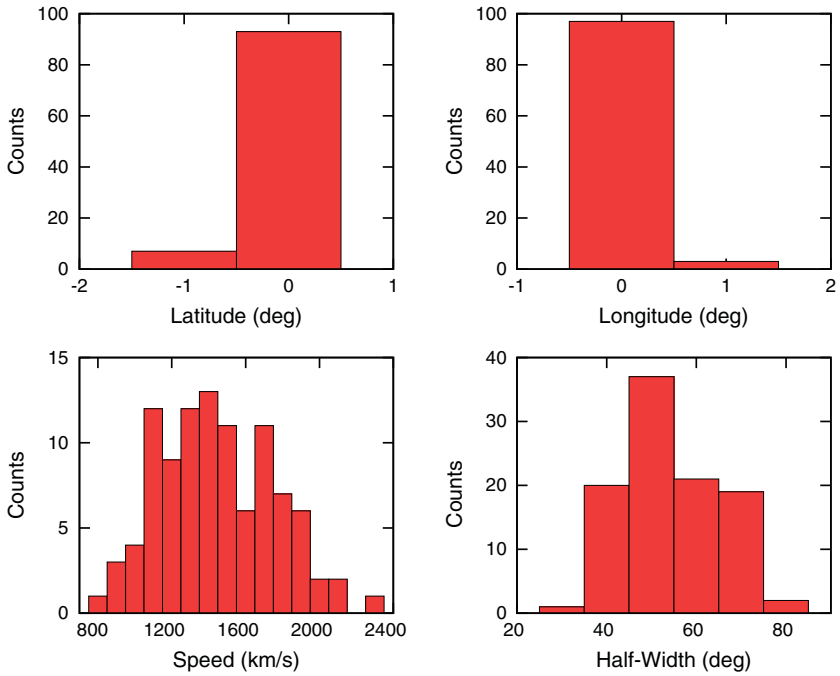

Figure 2. The cone parameter distributions, derived from CONED Model version 1.3, for event 4 (29 March 2001 CME). The count number is the number of times a cone parameter was within the range of a bin, for the 100 sets of cone parameters.

[30] The average of the ensemble standard deviations was calculated to be 4.6 ± 0.7 h (Table 3). This quantification of the propagation time uncertainty was based strictly on the uncertainty in the initial conditions calculated from LASCO imagery of the particular CMEs. Another measure of the propagation time uncertainty was the range of the ensembles, which were averaged to obtain 22.2 ± 5.2 h. While this was too large of an uncertainty to be useful for operational forecasts, it was an important metric to analyze the overall performance of the ensemble forecasting technique. The quantification of the uncertainty provided an estimate of the widths of the ensembles and was not a measure of the forecast error.

[31] The ensemble forecasts for the eight events with actual propagation times between 27 h and 46 h were the most accurate of the 15 forecasts, with all of the absolute forecast errors less than 8 h (Figure 10). The forecast errors for the two fast CMEs, events 10 and 11 (28 October 2003 and 29 October 2003 CMEs), were around 9 h indicating that the CME speeds were underestimated. The absolute forecast errors for events with actual propagation times less than 46 h were all less than 10 h.

[32] The forecast errors for the slow CMEs, with actual propagation times over 46 h, were all less than -10 h. This indicated that the ensemble forecasts greatly underestimated the propagation times of the slower CMEs. For the events with actual propagation times greater than 50 h, the absolute forecast error increased as the actual propagation time increased. The slowest event (event 9) had an actual propagation time of 60 h and a forecast error of -25 h. The large forecasting errors for the slower CMEs were due the fact that CONED Model 1.3 was tuned to more accurately forecast faster (more significant from the space weather point of view) events following the *Falkenberg et al.* [2011] study, forcing the CONED Model to select faster speeds.

[33] The mean absolute forecast error, for the 15 CMEs, was calculated to be 9.1 ± 7.1 h (Table 3). While the set of events between this analysis and the *Taktakishvili et al.* [2011] analysis were not identical, the ensemble forecasting mean absolute forecast error was greater than the mean absolute error of 6.9 ± 4.2 h found by *Taktakishvili et al.* [2011] using single ENLIL runs with the analytical Cone Model but was less than the 11.2 ± 7.2 h mean absolute error found by *Taktakishvili et al.* [2011] using single ENLIL runs with the median values of the cone parameters derived from CONED Model version 1.0. It must be noted that the *Taktakishvili et al.* [2011] analysis focused on CMEs associated with particularly large geomagnetic storms, while this analysis included multiple CMEs that produced relatively weak geomagnetic storms ($K_p \leq 4$), which could be considered less significant from the space weather point of view. Therefore, the forecast errors may not be directly comparable between the analyses.

4.4. Maximum K_p Index

[34] The ensemble forecast tended to overestimate the magnitude of the impacts of the CMEs by forecasting a maximum K_p of 9 for all 15 CMEs using the completely southward magnetic field assumption (Figure 11). Of the

Table 2. The Average and Standard Deviation Time, and Maximum K_p Distributions, for Event 4 (29 March 2001 CME)

Parameter	Average	Standard Deviation	Minimum	Maximum	Range
Speed (km/s)	1444.3	304.9	848.0	2256.0	1408.0
Angular Half Width (deg)	53.8	10.3	33.0	82.0	49.0
Latitude (deg)	−0.1	0.3	−1.0	0.0	1.0
Longitude (deg)	0.0	0.2	0.0	1.0	1.0
Propagation time (hours)	36.4	5.8	26.8	57.3	30.5
Southward IMF K_p	9	–	7	9	2
Uniform clock angle K_p	7	–	4	8	4

15 CMEs, seven had an actual maximum K_p of 9, and three had an actual maximum K_p less than 5. The ensemble forecasts for 10 of the 15 CMEs had accuracy such that the actual maximum K_p was within the range of the ensemble. Of the eight events with actual maximum K_p indices less than 9, three forecasts contained the actual maximum K_p inside of the range of the ensemble.

[35] The average of the ensemble ranges, for the 15 events, was calculated to be 0.7 ± 1.3 (Table 3). The ensemble ranges were zero for all but four events due to the overestimation of the maximum K_p values and the fact that any maximum K_p calculation exceeding 9 was truncated to 9. This provided a quantification of the uncertainty in the maximum K_p calculations and was not a measure of the forecast error. The mean absolute forecast error, for all 15 events, was calculated to be 1.7 ± 2.1.

[36] The completely southward magnetic field maximum K_p forecast is displayed along with the propagation time, per event, in Figure 12. The events with the largest propagation time errors also had the largest maximum K_p errors. This was due to overestimations of the CME speeds for these particular events, which forecast the arrival times too early, and the maximum K_p indices too large.

[37] The maximum K_p forecasts for 8 of the 15 events were lowered by using a uniformly distributed clock angle, relative to the completely southward magnetic field forecasts (Figure 11). The forecasts for 9 of the 15 events had accuracy such that the actual maximum K_p was within the range of the ensemble. The forecasts for 4 of the 8 events with actual maximum K_p indices less than 9 had the actual maximum K_p within the range of the ensemble, which was slightly better than the 3 of 8 for the completely southward magnetic field forecasts. But, the forecasts using a uniformly distributed clock-angle tended to underestimate the maximum K_p indices for the events with actual maximum K_p indices of 9. The average of the ensemble ranges, for the 15 CMEs, was calculated to be 1.5 ± 1.4 (Table 3). The range was 0 for 4 of the events, compared to 11 events for the completely southward magnetic field forecasts.

[38] The mean absolute forecast error for the 15 CMEs using a uniformly distributed clock angle was calculated to be 1.8, which was slightly larger than the 1.7 calculated

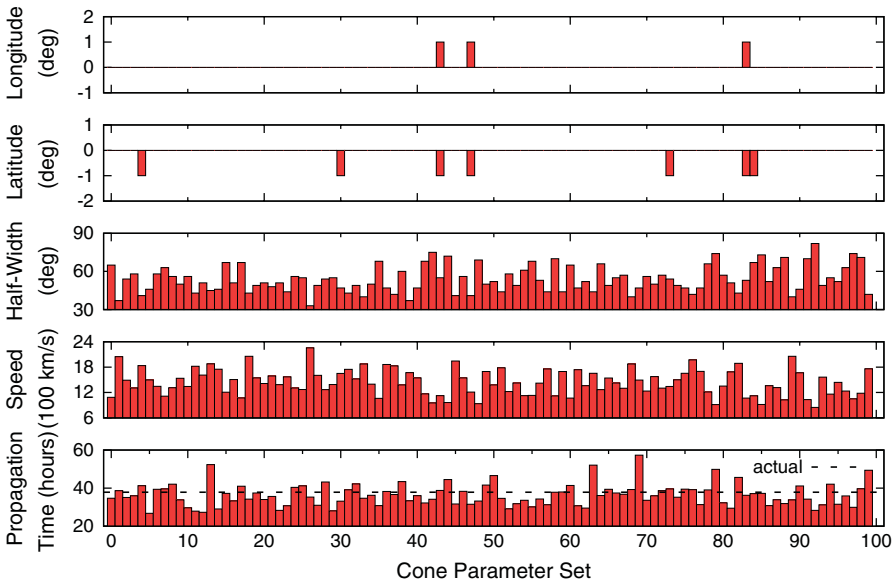

Figure 3. The cone parameters and propagation time forecasts for each of the 100 sets of parameters composing the ensemble for event 4 (29 March 2001 CME). Each set of cone parameters maps to a propagation time, which shows the relationship between the cone parameters and the ensemble forecast.

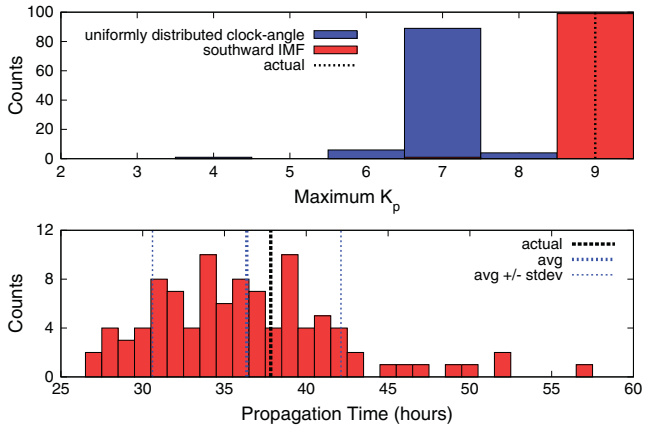

Figure 4. The maximum K_p index and propagation time ensemble forecasts, for event 4 (29 March 2001 CME). The count number is the number of times a cone parameter was within the range of a bin, for the 100 sets of forecasts derived from the 100 sets of cone parameters. The "southward IMF" describes the maximum K_p index calculations using a completely southward magnetic field, and the "uniformly distributed clock angle" describes the calculations using a uniformly distributed clock angle in the *Newell et al.* [2007] formula.

using the completely southward magnetic field forecasts. The mean absolute forecast error for the events with actual maximum K_p indices of 9 was 0.7, which was greater than the 0.0 for the completely southward magnetic field forecasts. The mean absolute forecast error for the events with actual maximum K_p indices less than 9 was 2.8, which was less than the 3.1 for the completely southward magnetic field forecasts. This indicated that the forecasts completed using a uniformly distributed clock angle were less accurate than the forecasts completed using a completely southward magnetic field for the events with actual maximum K_p indices of 9 but were more accurate for the events with actual maximum K_p indices less than 9. This follows from the fact that the magnetic field orientation of the CMEs that produced the weak geomagnetic storms were not conducive to producing large geomagnetic storms (there was not a large southward component), and the assumption that the magnetic field was completely southward tended to overestimate the magnitude of the K_p for these events.

[39] Using ACE data in the *Newell et al.* [2007] formula, along with the 6 h integration time described by *Newell et al.* [2007] (with SOHO Proton Monitor data to estimate the solar wind speed for events 8, 10, and 11, which had missing solar wind speed information from ACE due to proton events), the mean absolute error for the 15 events was calculated to be 0.5. This indicated that the *Newell et al.* [2007] formula used with actual solar wind data (including magnetic field orientation) as input could produce accurate K_p estimates. Therefore, the main source of the errors in the maximum K_p estimations from WSA-ENLIL with CONED Model were due to errors in the estimations of the solar

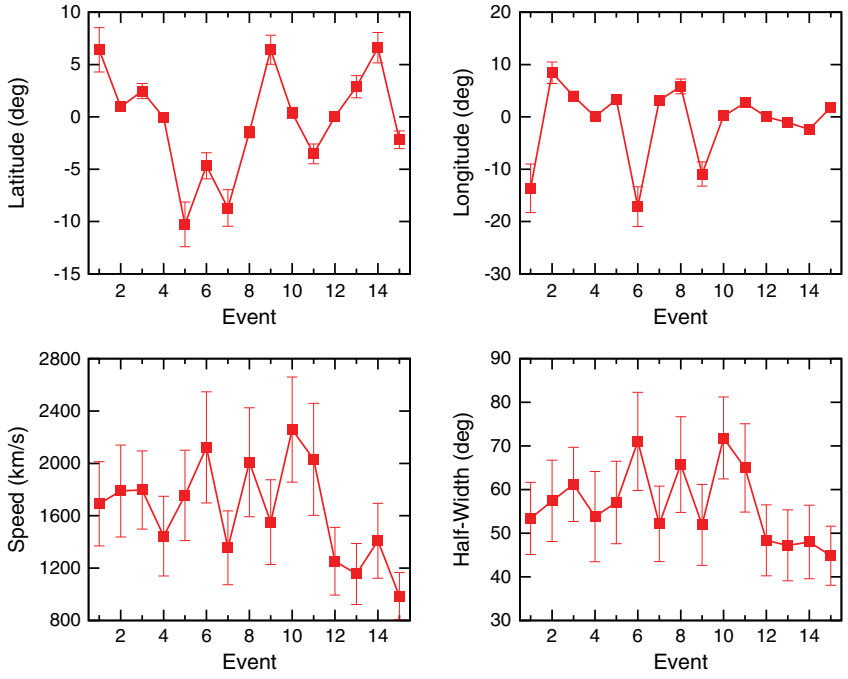

Figure 5. The average and standard deviation of the cone parameter distributions, derived from CONED Model version 1.3, for each event. The CONED Model used three LASCO C3 images of the CME eruption to develop the distributions of cone parameters, for each CME.

Table 3. The Averages of the Standard Deviations, Ranges, and Forecast Errors for the Cone Parameter, Propagation Time, and Maximum K_p Distributions, Over All 15 Event

Parameter	Average of the Standard Deviations	Average of the Ranges	Average of the Forecast Errors
Speed (km/s)	323.6	1568.3	–
Angular Half Width (deg)	9.1	43.3	–
Latitude (deg)	1.0	5.3	–
Longitude (deg)	1.3	6.8	–
Propagation time (hours)	4.6	22.2	9.1
Southward IMF K_p	–	0.7	1.7
Uniform clock angle K_p	–	1.5	1.8

wind parameters near Earth and the fact that no magnetic field orientation information was available.

5. Conclusions

[40] Ensemble simulations of CME impact and propagation to Earth were produced for 15 halo CMEs using the WSA-ENLIL version 2.7 with CONED Model version 1.3, helping to close the gap between terrestrial and space weather forecasting. The ensemble forecasts consisted of the propagation times to the L_1 Lagrangian point and the associated maximum K_p indices due to the impact of the CMEs on the Earth's magnetosphere. The ensemble forecasts were formed by using 100 sets of cone parameters, derived from LASCO C3 imagery via the CONED Model, as input to WSA-ENLIL to produce propagation time and maximum K_p index distributions.

[41] The propagation time ensemble forecasts estimated 5 of 15 events with accuracy such that the actual propagation time was within the ensemble average plus or minus the ensemble standard deviation. The forecasts for 8 of 15 events had accuracy such that the actual propagation time was within the range of the ensemble. The mean absolute forecast error, for the 15 CMEs, was calculated to be 9.1 h. The majority of the error came from the slow events because CONED Model 1.3 was tuned to more accurately forecast faster events following the *Falkenberg et al.* [2011] study.

[42] Perhaps the most important result of this analysis was the dynamic quantification of the forecast uncertainty derived strictly from measurements (LASCO imagery) of particular CMEs. The average of the propagation time standard deviations, over all 15 events, was calculated to be 4.6 h, and the average of the ensemble ranges was

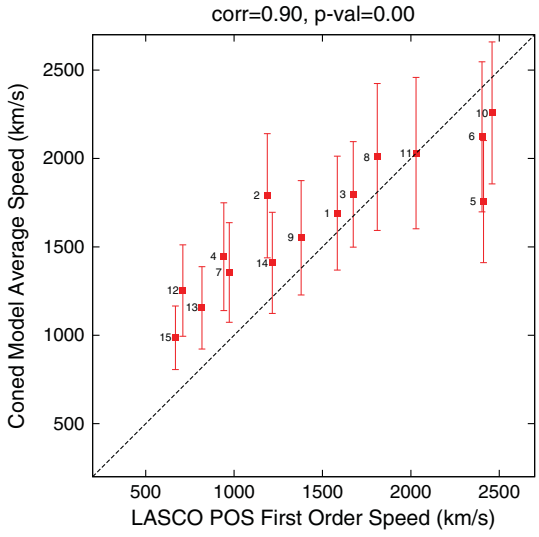

Figure 6. The CONED Model average speeds versus the LASCO first-order POS speeds, with the event number as the label and the standard deviations of the ensembles as the error bars. The two methods of calculating the CME speeds were strongly correlated, with the average ratio of the CONED Model average speeds to the LASCO first-order POS speeds calculated to be 1.2.

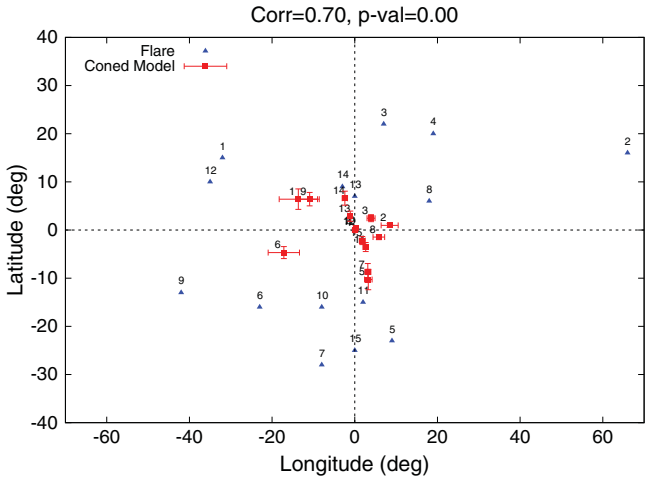

Figure 7. The CONED Model average longitudes and latitudes along with the associated solar flare latitudes and longitudes, with the event numbers as the labels and the standard deviations of the ensembles as the error bars. Relative to the associated solar flare locations, the CONED Model propagation axes tended to be pushed towards the Sun-Earth line.

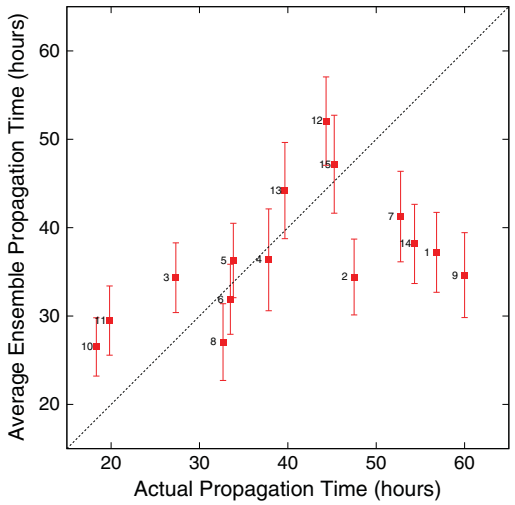

Figure 8. The averages and standard deviations of the propagation time ensembles versus the actual propagation times, with the event number as the label. The actual propagation time was within the average plus or minus one standard deviation for 5 of the 15 events.

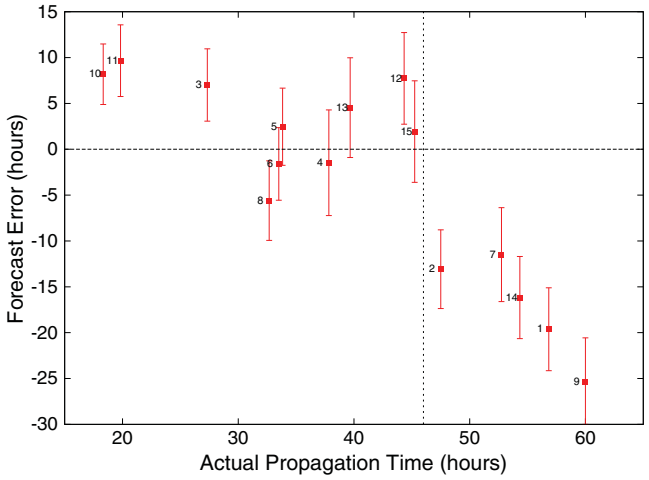

Figure 10. The propagation time forecast error versus the actual propagation time, with the error bars as one standard deviation and the labels as the event number. The forecasts for the events with actual propagation times between 27 and 46 h were the most accurate, while the largest forecast errors were for the events with actual propagation times greater than 46 h.

calculated to be 22.2 h. While these values were not a measure of the forecast accuracy, they did provide a measure of the uncertainty in the forecasts based on the uncertainty in the measurements of the initial conditions, which would be useful information in operational forecasts of CMEs.

[43] The maximum K_p indices were calculated using the maximum K_p index formula created by *Newell et al.* [2007] using two different magnetic field orientations. Using the completely southward magnetic field, the ensemble forecast predicted maximum K_p indices of 9 for all events, which was an overestimation for many of the events. The forecasts for 10 of the 15 events had accuracy such that the actual maximum K_p index was within the range of the ensemble forecast. The mean absolute forecast error was calculated to be 1.7, and the average of the ensemble ranges was 0.7.

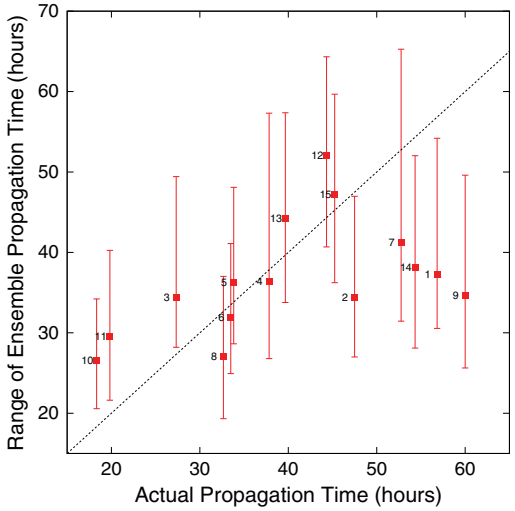

Figure 9. The averages and ranges of the propagation time ensembles versus the actual propagation times, with the event number as the label. The actual propagation time was within the ensemble range for 8 of the 15 events.

[44] Using a uniformly distributed clock angle, 9 of the 15 events were forecast with accuracy such that the actual maximum K_p index was within the range of the ensemble. The mean absolute forecast error was calculated to be 1.8, and the average of the ensemble ranges was 1.5. The forecasts using a uniformly distributed clock angle were more accurate than the forecasts assuming the magnetic field was completely southward for the events with actual maximum K_p indices less than 9 but were less accurate for the events with actual maximum K_p indices of 9.

[45] The next step in ensemble forecasting of CMEs is to advance the CONED Model to produce more accurate estimations of the initial CME parameters. Recently, *Jacobs et al.* [2012] developed more advanced segmentation techniques to use in the model. The current model development is focused on allowing the model to process multiple transients in the field of view and allowing the location of the CME eruption (associated solar flare location) as well as any propagation information derived from STEREO to be taken into account when calculating the cone parameters. Improvements in the estimations of the cone parameters should improve the overall accuracy of the ensemble forecasting technique.

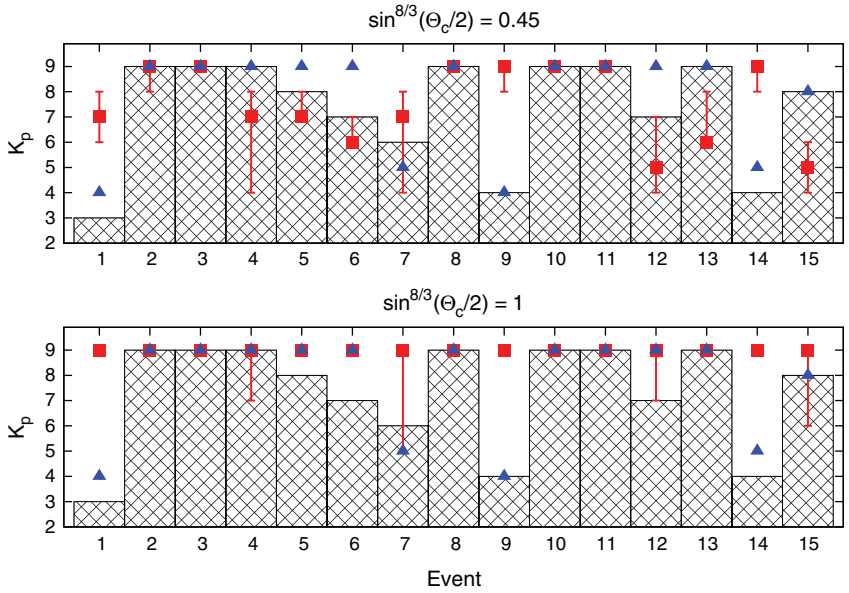

Figure 11. The average and range of the maximum K_p ensembles, per event, using a uniformly distributed clock angle in the *Newell et al.* [2007] formula (top) and the assumption that the magnetic field is completely southward (bottom). The red squares with error bars are the ensemble forecasts, the bars are the actual maximum K_p indices, and the blue triangles are the calculated maximum K_p indices using ACE solar wind data in the *Newell et al.* [2007] formula.

[46] Additionally, the K_p forecasts will be recalculated using the actual magnetic field orientations of the CMEs along with the WSA-ENLIL with CONED Model data to determine the improvement in the forecast accuracy if the actual magnetic field information was available. This will help determine the usefulness of accurate clock-angle estimates for K_p forecasts using the WSA-ENLIL with CONED Model.

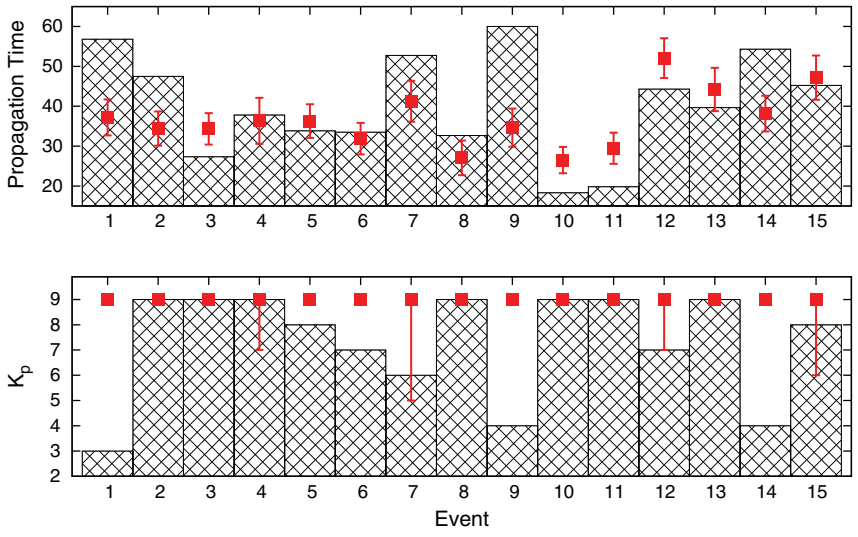

Figure 12. The average and range of the maximum K_p index ensemble using the completely southward magnetic field assumption, along with the average and standard deviation of the propagation time, per event, for the 15 CMEs. The ensemble forecasts and uncertainties are the points with the error bars, and the bars are the actual values. The events with the largest propagation time errors also had the largest maximum K_p errors, which was due to overestimations of the CME speeds.

[47] **Acknowledgments.** This analysis was sponsored by the Air Force Institute of Technology and the Community Coordinated Modeling Center. D. Emmons was sponsored by the Air Force Institute of Technology. The authors would like to thank NOAA/SWPC's warehouse, NASA's OMNIWeb and CDAW data centers, and the CELIAS/MTOF Proton Monitor (http://umtof.umd.edu/pm/) for the use of their data. The views expressed in this article are those of the authors and do not necessarily reflect the official policy or position of the Air Force, the Department of Defense, or the U.S. government.

References

Afraimovich, E., V. Demyanov, and T. Kondakova (2003), Degradation of GPS performance in geomagnetically disturbed conditions, *GPS Solutions*, *7*(2), 109–119.

Arge, C., and V. Pizzo (2000), Improvement in the prediction of solar wind conditions using near-real time solar magnetic field updates, *J. Geophys. Res.*, *105*, 10.

Boteler, D., R. Pirjola, and H. Nevanlinna (1998), The effects of geomagnetic disturbances on electrical systems at the Earth's surface, *Adv. Space Res.*, *22*(1), 17–27.

DelSole, T. (2005), Predictability and information theory. Part II: Imperfect forecasts, *J. Atmos. Sci.*, *62*(9), 3368–3381.

Dryer, M. (1974), Interplanetary shock waves generated by solar flares, *Space Sci. Rev.*, *15*(4), 403–468.

Falkenberg, T., A. Taktakishvili, A. Pulkkinen, S. Vennerstrom, D. Odstrcil, D. Brain, G. Delory, and D. Mitchell (2011), Evaluating predictions of ICME arrival at earth and mars, *Space Weather*, *9*(9), S00E12.

Fry, C., W. Sun, C. Deehr, M. Dryer, Z. Smith, S. Akasofu, M. Tokumaru, and M. Kojima (2001), Improvements to the HAF solar wind model for space weather predictions, *J. Geophys. Res.*, *106*(A10), 20,985–21.

Gopalswamy, N., A. Lara, S. Yashiro, M. Kaiser, and R. Howard (2001), Predicting the 1-AU arrival times of coronal mass ejections, *J. Geophys. Res.*, *106*(A12), 29,207–29,217, doi:10.1029/2001JA000177.

Gosling, J. (1993), The solar flare myth, *J. Geophys. Res.*, *98*(A11), 18,937–18.

Hakamada, K., and S. Akasofu (1982), Simulation of three-dimensional solar wind disturbances and resulting geomagnetic storms, *Space Sci. Rev.*, *31*(1), 3–70.

Jacobs, M., A. Pulkkinen, and L. Chang (2012), Improving coronal mass ejection segmentation using pattern recognition techniques, in *Proceedings of Image Processing, Computer Vision, and Pattern Recognition*, Las Vegas, NV, USA.

Leith, C. (1974), Theoretical skill of Monte Carlo forecasts (stochastic atmospheric processes), *Mon. Weather. Rev.*, *102*, 409–418.

Newell, P., T. Sotirelis, K. Liou, C. Meng, and F. Rich (2007), A nearly universal solar wind-magnetosphere coupling function inferred from 10 magnetospheric state variables, *J. Geophys. Res.*, *112*, 1–16.

Odstrčil, D., and V. Pizzo (1999), Three-dimensional propagation of coronal mass ejections (CMEs) in a structured solar wind flow 1. CME launched within the streamer belt, *J. Geophys. Res.*, *104*(A1), 483–492.

Odstrcil, D., P. Riley, and X. Zhao (2004), Numerical simulation of the 12 May 1997 interplanetary CME event, *J. Geophys. Res.*, *109*, A02116.

Pulkkinen, A., T. Oates, and A. Taktakishvili (2010), Automatic determination of the conic coronal mass ejection model parameters, *Sol. Phys.*, *261*(1), 115–126.

Smith, Z., and M. Dryer (1990), MHD study of temporal and spatial evolution of simulated interplanetary shocks in the ecliptic plane within 1 au, *Sol. Phys.*, *129*(2), 387–405.

Taktakishvili, A., M. Kuznetsova, P. MacNeice, M. Hesse, L. Rastatter, A. Pulkkinen, A. Chulaki, and D. Odstrcil (2009), Validation of the coronal mass ejection predictions at the earth orbit estimated by ENLIL heliosphere cone model, *Space Weather*, *7*, S03004, doi:10.1029/2008SW000448.

Taktakishvili, A., P. MacNeice, and D. Odstrcil (2010), Model uncertainties in predictions of arrival of coronal mass ejections at earth orbit, *Space Weather*, *8*(6), S06007.

Taktakishvili, A., A. Pulkkinen, P. MacNeice, M. Kuznetsova, M. Hesse, and D. Odstrcil (2011), Modeling of coronal mass ejections that caused particularly large geomagnetic storms using ENLIL heliosphere cone model, *Space Weather*, *9*(6), S06002.

Tóth, G., and D. Odstrcil (1996), Comparison of some flux corrected transport and total variation diminishing numerical schemes for hydrodynamic and magnetohydrodynamic problems, *J. Comput. Phys.*, *128*(1), 82–100.

Xie, H., L. Ofman, and G. Lawrence (2004), Cone model for halo CMEs: Application to space weather forecasting, *J. Geophys. Res.*, *109*(A3), A03109.

Zhao, X., S. Plunkett, and W. Liu (2002), Determination of geometrical and kinematical properties of halo coronal mass ejections using the cone model, *J. Geophys. Res.*, *107*(1223), 10–1029.